Publ. Astron. Soc. Japan (2018) 70 (5), 94 (1–10)
doi: 10.1093/pasj/psy092
Advance Access Publication Date: 2018 September 19

LAMOST J221750.59+210437.2: A new member of carbon-enhanced extremely metal-poor stars with excesses of Mg and Si

Wako Aoki,[1,2] Tadafumi Matsuno,[2] Satoshi Honda,[3] Miho N. Ishigaki,[4] Haining Li,[5] Takuma Suda,[6] and Yerra Bharat Kumar[5]

[1]National Astronomical Observatory, 2-21-1 Osawa, Mitaka, Tokyo 181-8588, Japan
[2]Department of Astronomical Science, School of Physical Sciences, The Graduate University of Advanced Studies (SOKENDAI), 2-21-1 Osawa, Mitaka, Tokyo 181-8588, Japan
[3]Center for Astronomy, University of Hyogo, 407-2 Nishigaichi, Sayo-cho, Sayo, Hyogo 679-5313, Japan
[4]Kavli Institute for the Physics and Mathematics of the Universe (WPI), The University of Tokyo, 5-1-5 Kashiwanoha, Kashiwa, Chiba 277-8583, Japan
[5]Key Lab of Optical Astronomy, National Astronomical Observatories, Chinese Academy of Sciences, A20 Datun Road, Chaoyang, Beijing 100012, China
[6]Research Center for the Early Universe, Graduate School of Science, The University of Tokyo, 7-3-1 Hongo, Bunkyo-ku, Tokyo 113-0033, Japan

*E-mail: aoki.wako@nao.ac.jp

Received 2018 June 8; Accepted 2018 July 18

Abstract

We report on the elemental abundances of the carbon-enhanced metal-poor (CEMP) star J2217+2104, discovered through our metal-poor star survey with LAMOST and Subaru. This object is a red giant and has extremely low Fe abundance ([Fe/H] = −4.0) and very large enhancement of C, N, and O with excesses of Na, Mg, Al, and Si. This star is a new example of a small group of such CEMP stars identified by previous studies. We find a very similar abundance pattern for O–Zn in this class of objects that shows enhancement of elements up to Si and normal abundance of Ca and Fe-group elements. Whereas the C/N ratio is different among these stars, the (C + N)/O ratio is similar. This suggests that similar abundance ratios of C were also yielded, relative to O–Zn in progenitors, and was later affected by the CN-cycle. By contrast, the heavy neutron-capture elements Sr and Ba are deficient in J2217+2104, compared to the four objects in this class previously studied. This indicates that the neutron-capture process in the early Galaxy, presumably the r-process, has no direct connection to the phenomenon that has formed such CEMP stars. Comparisons of the abundance pattern that are well determined for such CEMP stars with those of supernova nucleosynthesis models constrain the progenitor mass to be about 25 $M_{\odot}$, which is not particularly different from the typical mass of progenitors expected for extremely metal-poor stars in general.

Key words: nuclear reactions, nucleosynthesis, abundances — stars: abundances — stars: individual (LAMOST J221750.59+210437.2) — stars: Population II

1 Introduction

Extremely metal-poor (EMP) stars ([Fe/H] $\lesssim -3$) in the Milky Way are regarded as old low-mass stars formed in the very early stage of the Galaxy evolution preserving the yields of first generations of massive stars (Frebel & Norris 2015).[1] A remarkable feature found in EMP stars is the high frequency of carbon-enhanced metal-poor (CEMP) stars ([C/Fe] $> +0.7$).[2] A large fraction of CEMP stars with [Fe/H] > -3 also show excesses of heavy neutron-capture elements like Ba, a signature of contribution by the s-process nucleosynthesis in asymptotic giant branch (AGB) stars (Käppeler et al. 2011) through mass transfer across binary systems (so-called CEMP-s stars). By contrast, CEMP stars with no excess of Ba (CEMP-no stars) are dominant at [Fe/H] < -3 (e.g., Aoki et al. 2007). CEMP stars with such low metallicity could record the nucleosynthesis yields of a kind of supernova that is particularly effective in the early Galaxy. The high frequency of such objects could also be related to the cooling process of star-forming clouds. The excess of C, as well as O that is also overabundant in some CEMP stars, could result in efficient gas cooling, which is required for low-mass star formation, even at very low metallicity (Bromm & Loeb 2003; Norris et al. 2013).

Most of the CEMP-no stars do not show any anomaly in abundance ratios except for the light elements C, N, and O (e.g., Aoki et al. 2007; Ito et al. 2009). The [C/Fe] values of the CEMP-no stars show a wide distribution, including many objects that have a ratio close to the criterion of CEMP stars ([C/Fe] $\sim +1$; Yoon et al. 2016). These observational features could suggest a connection of some fraction of CEMP-no stars with C-normal stars.

There are, however, a small number of CEMP-no stars that show large excesses of some α-elements, which separates them well from C-normal EMP stars. The first example of such a star, CS 22949−037, was reported by McWilliam et al. (1995), and was studied in more detail by Norris, Ryan, and Beers (2001), Norris et al. (2002), and Depagne et al. (2002). This is a CEMP star with [Fe/H] ~ -4 showing no significant excess of neutron-capture elements, but it exhibits clear excesses of Mg and Si, as well as odd elements with similar atomic mass (Na, Al). Another EMP star having a similar abundance pattern, CS 29498−043 ([Fe/H] ~ -3.5), was reported by Aoki et al. (2002), who suggested the existence of a class of CEMP-no stars with significant excesses of Mg and Si in the lowest metallicity range. Two more CEMP-no stars that have similarly large excess of Mg and Si have been reported by Cohen et al. (2013) and Yong et al. (2013): HE 1012−1510 ([Fe/H] $= -3.5$) and HE 2139−5432 ([Fe/H] $= -4.0$). More recently, Bonifacio et al. (2018) reported another EMP star, SDSS J1349+1407, that has [Fe/H] $= -3.6$ and large excesses of C, Na, and Mg, although the number of elements for which abundances are measured is still small for this faint, unevolved object. These stars are well separated from other stars with similar Fe abundances in the α/Fe abundance ratios (e.g., [Mg/Fe]; Norris et al. 2013). Given the fact that α-elements are efficiently produced during the evolution of massive stars and their supernova explosions, these CEMP stars could be regarded as a record of nucleosynthesis by the first generation of massive stars.

Large excesses of C, N, O, and Mg are also found in the "hyper metal-poor" ([Fe/H] < -5) star HE 1327−2326 (Frebel et al. 2005). Although the overabundances of C, N, and O are much more significant in this object than in the above CEMP stars, the overall abundance trend could suggest that these stars have similar origins.

The distributions of abundance ratios for CEMP-no stars were discussed in detail by Norris et al. (2013), upon which stars with excesses of Na, Mg, and Si are focused. As possible origins of these objects, so-called faint supernovae explained by the "mixing fall-back" models (Umeda & Nomoto 2003) and mass-loss from rotating massive stars (Meynet et al. 2006) are argued. To discriminate between these possibilities, detailed abundance pattern of α-elements up to Ti is a key. The sample of such stars is, however, still very limited, as mentioned above, even though EMP stars have been intensively searched for in the past two decades. This could be due to the fact that such EMP stars ([Fe/H] $\lesssim -3.5$) are generally very rare. Taking account of the importance of such objects in the understanding of formation and evolution of the first generations of stars, further searches for new examples and detailed abundance studies are desired.

Here we report on the discovery of an ultra metal-poor (UMP; [Fe/H] $\lesssim -4$) star, LAMOST J221750.59+210437.2 (hereafter, J2217+2104), which shows large excesses of α-elements as well as C, and we discuss the detailed abundance pattern of this class of objects.

2 Observations and measurements

J2217+2104 was discovered via medium-resolution ($R \sim 1800$) spectroscopy with the Large Sky Area Multi-Object Fiber Spectroscopic Telescope (LAMOST) in its regular survey (Cui et al. 2012; Zhao et al. 2012) as a candidate the EMP stars. The stellar parameters estimated from the LAMOST spectrum indicate that this object is an EMP giant with [Fe/H] < -3.5. Strong CH molecular bands are identified in the LAMOST spectrum.

[1] [A/B] $= \log(N_A/N_B) - \log(N_A/N_B)_\odot$, and $\log \epsilon_A = \log(N_A/N_H) + 12$ for elements A and B.

[2] We adopt [C/Fe] $> +0.7$ as the definition of CEMP stars in this paper following the definition of SAGA database (Suda et al. 2008), whereas [C/Fe] $> +1.0$ is adopted in some other papers.

Table 1. Observations and radial velocities.

Facility (resolving power)	Obs. date	HJD*	Wavelengths (Å)	S/N	$V_{\rm Helio}$ (km s^{-1})†
LAMOST ($R = 2000$)	2013 Oct. 23	2456588	3800–9000	—	− 116.7
Subaru ($R = 45000$)	2015 Nov. 30	2457356.77	4030–6800	40	− 115.79
Subaru ($R = 60000$)	2017 Aug. 4	2457970.00	3500–5300	61	− 116.13
Subaru ($R = 60000$)	2017 Aug. 5	2457971.00	4030–6800	26	− 115.29
Gaia DR2					− 117.7

*Heliocentric Julian Date.
†The heliocentric radial velocity errors of LAMOST and Gaia results are 7 km s^{-1} and 3.3 km s^{-1}, respectively.

High-resolution spectra of this object were obtained with the Subaru Telescope High Dispersion Spectrograph (HDS: Noguchi et al. 2002) in observing programs for follow-up spectroscopy of metal-poor star candidates found with LAMOST (Li et al. 2015). The first spectrum was obtained in 2015 November with a short exposure (so-called "snapshot" spectroscopy). High-resolution spectra with longer exposures were obtained in 2017 August with a resolving power of $R = 60000$ by two wavelength setups, covering 3500–5200 Å and 4030–6800 Å. Details of the observations are given in table 1.

Standard data reduction procedures were carried out with the IRAF echelle package.[3] The wavelength shift due to Earth's orbital motion is corrected using the IRAF task *rvcor*.

We measure equivalent widths by fitting a Gaussian profile. Line data for spectral features are taken from previous studies on very metal-poor stars (e.g., Aoki et al. 2013). The measured equivalent widths are given in table 2, together with the line data used in the abundance analysis.

The Fe I lines for which equivalent widths are measured are also used to measure radial velocities. The heliocentric radial velocities derived from these Fe I lines are given in table 1. The random error in the measurement is estimated to be $\sigma_v N^{-1/2}$, where σ_v is the standard deviation of the derived values from individual lines, and N is the number of lines used. The random errors are 0.03–0.04 km s^{-1}. The errors due to the instability of the instrument corresponding to, e.g., temperature variations, are usually larger ($\sim$0.5 km s^{-1}) than the above errors. The radial velocity obtained from the LAMOST spectrum and the value provided by Gaia Data Release 2 (DR2) are also given in the table. Given the errors of radial velocity measurements, no signature of radial velocity variation is found in the data currently available.

Photometry data ($B = 14.697$, $V = 13.388$, $J = 11.304$, and $K = 10.644$) are taken from AAVSO Photometric All-Sky Survey (APASS: Henden et al. 2016) and Two Micron All Sky Survey (2MASS: Cutri et al. 2003). The V magnitude of this object indicates that this is the brightest CEMP star with a large excess of Mg and Si known todate.

The parallax provided by the Gaia DR2 (0.0004 ± 0.0259 mas) is still uncertain and is not useful for constraining the distance or surface gravity.

[3] IRAF is distributed by the National Optical Astronomy Observatories, which is operated by the Association of Universities for Research in Astronomy, Inc. under cooperative agreement with the National Science Foundation.

3 Abundance analysis and results

We determine the elemental abundances of J2217+2104 by 1D/local thermodynaic equilibrium (LTE) standard analysis and spectrum synthesis techniques using model atmospheres of the ATLAS NEWODF grid (Castelli et al. 1997). To determine the stellar parameters, photometry is also used.

3.1 Stellar parameters and abundance analysis

We estimate the effective temperature ($T_{\rm eff}$) from the colors using the temperature scale of Alonso, Arribas, and Martínez-Roger (1999) for giant stars. We assume [Fe/H] $= -3$ in the calculation of $T_{\rm eff}$, following Ryan, Norris, and Beers (1999). The reddening [$E(B - V) = 0.054$] is adopted from Schlafly and Finkbeiner (2011). The derived $T_{\rm eff}$ from $(V - K)_0$ is 4494 K, which agrees with those from $(B - V)_0$ (4567 K) and from $(J - K)_0$ (4615 K) within the uncertainties of the estimates. We adopt $T_{\rm eff} = 4500$ K in the abundance analysis, taking account of the sensitivity of $V - K$ to $T_{\rm eff}$ and the uncertainty due to errors of photometry data and the temperature scale.

The surface gravity (g) and micro-turbulent velocity ($v_{\rm turb}$) are determined following the usual abundance analysis procedure, as the Fe abundances derived from Fe I and Fe II lines are consistent, and as there remains no trend of Fe abundances from individual Fe I lines as a function of the line strengths, respectively. For the analysis, 53 Fe I lines and four Fe II lines are used. Errors in the Fe abundance measurements of 0.1 dex results in an uncertainty in $\log g$ of 0.2 dex. The derived $\log g$ and $v_{\rm turb}$ are 0.9 dex and 2.3 km s^{-1}, respectively.

The derived Fe abundances from individual Fe I lines show a correlation with a lower excitation potential (χ):

Table 2. Atomic line data, equivalent widths and derived abundances.

Species	Wavelength (Å)	χ (eV)	log gf	W (mÅ)	log ϵ
Na I	5889.95	0.000	0.10	173.8	3.68
Na I	5895.92	0.000	−0.20	151.4	3.60
Mg I	4571.10	0.000	−5.69	80.5	5.19
Mg I	4702.99	4.330	−0.44	60.7	4.99
Mg I	5172.68	2.712	−0.45	195.4	5.23
Mg I	5183.60	2.717	−0.24	216.1	5.23
Mg I	5528.40	4.346	−0.50	62.6	5.04
Al I	3961.52	0.014	−0.34	136.7	3.12
Si I	4102.94	1.909	−3.14	48.5	4.46
Ca I	4226.73	0.000	0.24	134.6	2.63
Ca I	4454.78	1.898	0.26	21.3	2.51
Sc II	4246.82*	0.315	0.24	102.8	−0.45
Sc II	4320.75*	0.605	−0.25	35.7	−0.84
Sc II	4415.56*	0.595	−0.67	22.2	−0.73
Ti I	4991.07	0.836	0.45	10.3	1.13
Ti II	4417.72	1.165	−1.19	33.2	1.14
Ti II	4443.80	1.080	−0.71	61.5	1.04
Ti II	4450.48	1.084	−1.52	24.6	1.18
Ti II	4464.45	1.161	−1.81	10.9	1.14
Ti II	4468.49	1.131	−0.63	63.0	1.05
Ti II	4501.27	1.116	−0.77	51.9	0.98
Ti II	4533.97	1.237	−0.77	65.2	1.35
Ti II	4563.77	1.221	−0.96	50.8	1.27
Ti II	4571.97	1.572	−0.31	48.4	1.02
Cr I	4289.72	0.000	−0.37	62.7	1.30
Cr I	5206.04	0.941	0.02	23.2	1.27
Cr I	5208.42	0.941	0.17	33.7	1.34
Mn I	4033.06*	0.000	−0.65	58.6	0.67
Fe I	4063.59	1.558	0.06	104.9	3.29
Fe I	4071.74	1.608	−0.01	104.2	3.40
Fe I	4132.06	1.608	−0.68	85.9	3.58
Fe I	4143.42	3.047	−0.20	15.7	3.37
Fe I	4143.42	3.047	−0.20	15.7	3.51
Fe I	4147.67	1.485	−2.10	22.2	3.53
Fe I	4216.18	0.000	−3.36	70.1	3.84
Fe I	4250.79	1.557	−0.71	72.6	3.21
Fe I	4260.47	2.399	0.08	73.7	3.50
Fe I	4271.76	1.485	−0.17	112.2	3.53
Fe I	4282.40	2.176	−0.78	41.0	3.45
Fe I	4337.05	1.557	−1.70	38.1	3.54
Fe I	4375.93	0.000	−3.02	85.4	3.79
Fe I	4383.54	1.485	0.21	118.5	3.27
Fe I	4404.75	1.557	−0.15	104.6	3.36
Fe I	4415.12	1.608	−0.62	89.1	3.51
Fe I	4427.31	0.052	−2.92	98.8	4.07
Fe I	4442.34	2.198	−1.25	30.4	3.74
Fe I	4459.12	2.176	−1.28	24.2	3.60
Fe I	4461.65	0.087	−3.21	77.8	3.91
Fe I	4489.74	0.121	−3.97	29.0	3.82
Fe I	4494.56	2.198	−1.14	24.5	3.49
Fe I	4528.61	2.176	−0.82	40.7	3.47
Fe I	4531.15	1.485	−2.15	24.8	3.62
Fe I	4602.94	1.485	−2.21	23.4	3.64
Fe I	4871.32	2.865	−0.36	19.4	3.38
Fe I	4890.75	2.876	−0.39	16.2	3.33
Fe I	4891.49	2.851	−0.11	22.9	3.21
Fe I	4918.99	2.865	−0.34	22.3	3.43
Fe I	4920.50	2.833	0.07	43.5	3.41
Fe I	4957.60	2.808	0.23	54.4	3.40
Fe I	4994.13	0.915	−2.96	21.9	3.61
Fe I	5006.12	2.833	−0.61	17.8	3.54
Fe I	5012.07	0.859	−2.64	45.6	3.68
Fe I	5041.07	0.958	−3.09	20.2	3.75
Fe I	5041.76	1.485	−2.20	25.2	3.64
Fe I	5051.63	0.915	−2.80	36.3	3.74
Fe I	5083.34	0.958	−2.96	25.8	3.74
Fe I	5123.72	1.011	−3.07	16.9	3.69
Fe I	5127.36	0.915	−3.31	12.4	3.65
Fe I	5142.93	0.958	−3.08	16.3	3.62
Fe I	5151.91	1.011	−3.32	12.7	3.80
Fe I	5171.60	1.485	−1.79	43.7	3.57
Fe I	5192.34	2.998	−0.42	16.3	3.50
Fe I	5194.94	1.557	−2.09	25.6	3.62
Fe I	5216.27	1.608	−2.15	16.9	3.52
Fe I	5227.19	1.557	−1.23	73.4	3.58
Fe I	5232.94	2.940	−0.06	30.9	3.42
Fe I	5254.96	0.110	−4.76	8.7	3.91
Fe I	5269.54	0.860	−1.32	121.3	3.76
Fe I	5270.36	1.608	−1.51	61.4	3.72
Fe I	5324.18	3.211	−0.10	12.7	3.31
Fe I	5328.04	0.915	−1.47	110.5	3.72
Fe I	5328.04	0.915	−1.47	110.5	3.52
Fe I	5455.61	1.011	−2.10	71.2	3.69
Fe I	5497.52	1.011	−2.85	24.7	3.64
Fe I	5501.46	0.958	−3.05	17.9	3.61
Fe I	5506.78	0.990	−2.80	31.3	3.70
Fe I	5615.64	3.332	0.05	19.8	3.51
Fe I	6230.72	2.559	−1.28	9.9	3.50
Fe II	4522.63	2.844	−2.25	17.2	3.80
Fe II	4923.93	2.891	−1.26	36.6	3.29
Fe II	5018.45	2.891	−1.10	48.4	3.33
Fe II	5234.63	3.221	−2.18	11.8	3.96
Fe II	5316.62	3.153	−1.87	13.8	3.64
Co I	4118.77*	1.049	−0.48	41.2	1.56
Co I	4121.31*	0.922	−0.33	34.1	1.13
Ni I	5476.90	1.826	−0.78	23.0	2.26
Sr II	4077.71	0.000	0.15	53.6	−2.63
Sr II	4215.52	0.000	−0.18	59.6	−2.21
Ba II	4554.04	0.000	0.17	10.4	−2.21
Ba II	4934.09	0.000	−0.16	9.9	−2.21

*The effect of hyperfine splitting is included in the analysis.

δ[Fe/H]/$\delta\chi = -0.14\,\mathrm{dex\,eV^{-1}}$. The slope is shallower if the lines with the lowest excitation potential (<1 eV) are excluded. Such a trend is, however, usually found in the analysis of EMP giants adopting $T_{\rm eff}$ estimated from colors (e.g., Frebel et al. 2013). Hence, we adopt the $T_{\rm eff}$ estimated from the colors with no correction.

Table 3. Abundance results obtained for J2217+2104.

	$\log\epsilon$	n	$\log\epsilon\odot$	[X/Fe]	$\sigma_{[X/Fe]}$
C	5.55		8.43	1.03	0.2
N	6.10		7.83	2.18	0.3
O	6.90	1	8.69	2.12	0.2
Na	3.64	2	6.24	1.33	0.18
Mg	5.14	5	7.60	1.46	0.08
Al	3.12	1	6.45	0.60	0.2
Si	4.46	1	7.51	0.88	0.18
Ca	2.57	2	6.34	0.16	0.15
Sc II	−0.67	3	3.15	0.11	0.19
Ti I	1.13	1	4.95	0.11	0.19
Ti II	1.13	9	4.95	0.11	0.19
Cr I	1.30	3	5.64	−0.41	0.11
Mn	0.67	1	5.43	−0.83	0.19
Fe I	3.57	60	7.50	−3.93	0.17
Fe II	3.60	5	7.50	−3.90	0.24
Co	1.35	2	4.99	0.28	0.13
Ni	2.26	1	6.22	−0.04	0.18
Zn	<1.5		4.56	<0.8	
Sr	−2.42	2	2.87	−1.37	0.20
Ba	−3.36	2	2.18	−1.62	0.20
$^{12}C/^{13}C$	6^{+4}_{-2}	3	89	...	...

We estimate the uncertainties of $T_{\rm eff}$, $\log g$, [Fe/H], and $v_{\rm turb}$ to be 100 K, 0.3 dex, 0.3 dex, and 0.3 km s^{-1}, respectively, from the photometry errors and scatter of the Fe abundances derived from individual Fe lines.

3.2 Abundance analysis

The abundances of elements other than C and N listed in table 3 are determined by equivalent widths analysis. For the analysis of the Sc II, Mn I, Co I, and Ba II lines, the effect of hyperfine splitting is included, using the wavelengths and the fraction of transition probability of each split line in the Kurucz line data.[4] The isotope ratios of the solar-system r-process component are assumed for Ba. The effect is 0.11 dex in the Mn abundance, determined by a single line with moderate strength, whereas the effects are minor (0.02–0.03 dex) in the abundances of the other three elements.

The C and N abundances are determined by spectrum synthesis technique for the CH 4323 Å and CN 3883 Å bands, using the line lists of Masseron et al. (2014) for CH and Sneden et al. (2014) for CN. The wavelength range of the CH band is shown in figure 1.

The C isotope ratio ($^{12}C/^{13}C$) is estimated to be 6 from the CH molecular lines around 4000 Å. An example of the spectral feature is depicted in figure 1.

The O abundance is determined from the [O I] absorption line at 6300 Å. The stellar absorption line does not overlap with the telluric features ([O I] emission line and O_2 absorption lines; see Aoki et al. 2004) in the spectrum obtained on 2017 August 5. We measure the [O I] equivalent width with no correction of telluric features.

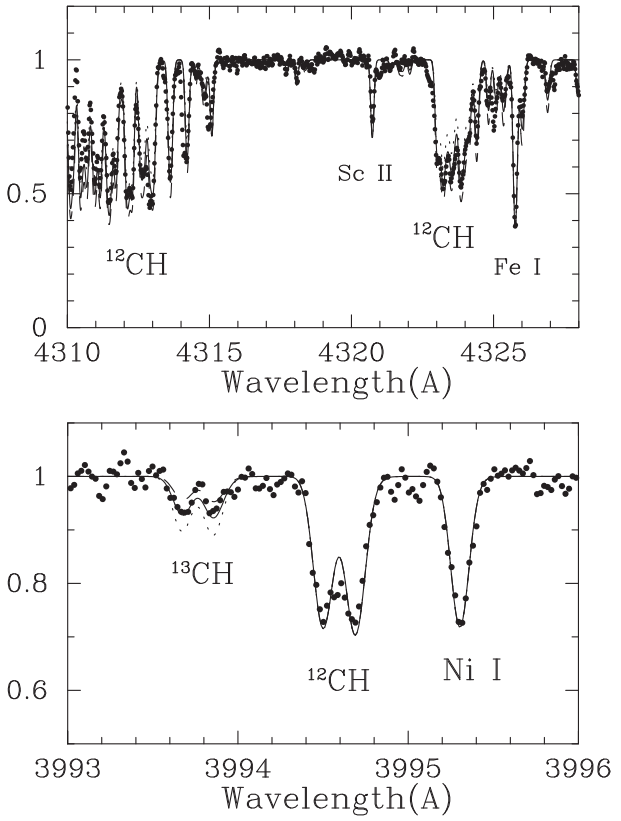

Fig. 1. Spectral features of CH molecule in J2217+2104. (upper) The CH absorption bands with synthetic spectra for [C/Fe] = 0.83 (dotted line), 1.03 (solid line), and 1.23 (dashed line). The ^{12}CH and ^{13}CH molecular lines around 3994 Å with synthetic spectra for $^{12}C/^{13}C = 4$ (dotted line), 6 (solid line), and 10 (dashed line).

No Zn I line is detected in the spectrum. The upper limit of Zn abundance ([Zn/Fe] < 0.8) is estimated from the Zn I 4722 Å line adopting an upper limit of the equivalent width of 3 mÅ at the 2σ level. We note that the Zn I 4811 Å line is not available in the spectrum due to bad CCD columns.

The results of the abundance measurements are given in table 3. The solar abundances of Asplund et al. (2009) are adopted to calculate the [X/Fe] values. The error of the abundance of each element is also given in the table. The error is obtained by adding in quadrature the random error and errors due to the uncertainties of stellar parameters. The random errors in the measurements are estimated to be $\sigma N^{-1/2}$, where σ is the standard deviation of derived abundances from individual lines, and N is the number of lines used. The σ of Fe I ($\sigma_{\rm Fe\,I}$) is adopted in the estimates for element X, for which the number of lines available in the analysis ($N_{\rm X}$) is small (i.e., the error is $\sigma_{\rm Fe\,I} N_{\rm X}^{-1/2}$). The errors due to the uncertainty of the atmospheric parameters

[4] ⟨http://kurucz.harvard.edu/linelists.html⟩.

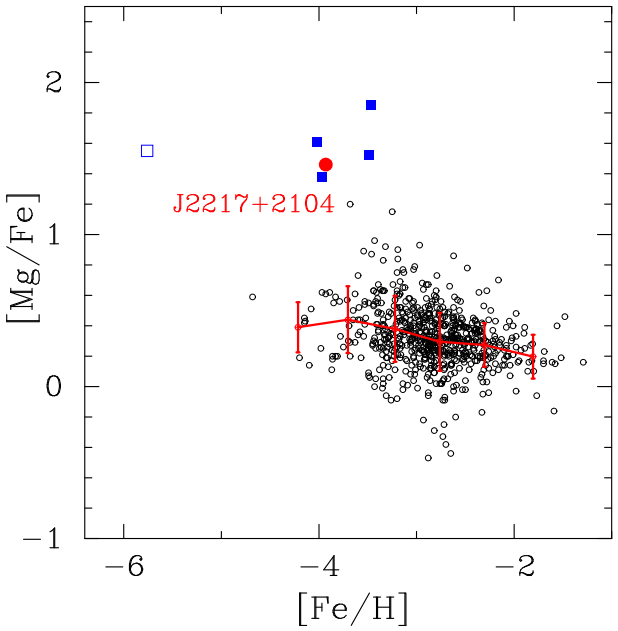

Fig. 2. [Mg/Fe] as a function of [Fe/H] for J2217+2104 (the red filled circle) and other stars. Abundance data of the four CEMP stars with excesses of Mg and Si (blue filled squares) and HE 1327−2326 (open square) are adopted from Norris et al. (2013). Abundance data of other stars (small circles) are taken from literature (see text). CEMP stars with excesses of neutron-capture elements, mostly CEMP-s stars, are excluded. The solid line and bars indicate averages and standard deviations of [Mg/Fe] values of 0.25 dex bins of [Fe/H]. In the calculations of the averages and standard deviations, the five CEMP stars with large excesses of Mg and Si are excluded. (Color online)

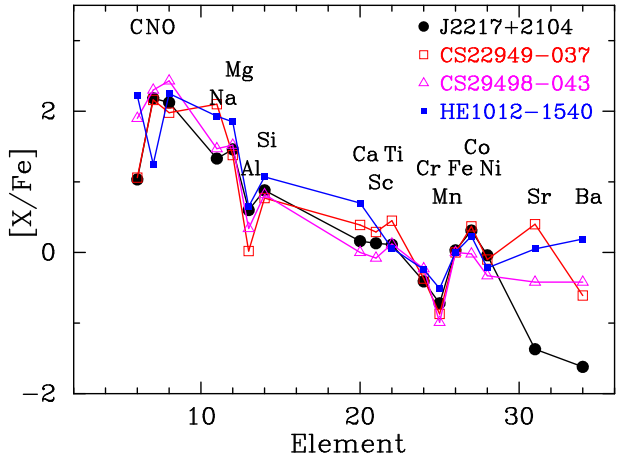

Fig. 3. Abundance patterns of four CEMP stars with large excesses of Mg and Si. The object names and corresponding symbols are presented in the panel. (Color online)

are estimated for a giant: $\delta T_{\rm eff} = 100$ K, $\delta \log g = 0.3$, and $\delta v_{\rm turb} = 0.3$ km s^{-1}. The errors due to uncertainties of stellar parameters are similar to the previous estimates for EMP giants (e.g., Aoki et al. 2004).

4 Discussion

4.1 Overall abundance pattern of CEMP stars with excesses of Mg and Si

Figure 2 shows the abundance ratios of [Mg/Fe] as a function of [Fe/H]. Abundance data of J2217+2104 and the other four CEMP stars with Mg excess (CS 22949−037, CS 29498−043, HE 1012−1540, and HE 2139−5432) are shown by the red filled circles and blue filled squares, respectively. The abundance data for the four objects are adopted from Norris et al. (2013), who compiled the results obtained by the analysis of Yong et al. (2013). The abundance data of the other stars (small circles) are taken from literature (Cayrel et al. 2004; Honda et al. 2004; Barklem et al. 2005; Lai et al. 2008; Aoki et al. 2013; Cohen et al. 2013; Yong et al. 2013; Hansen et al. 2015; Jacobson et al. 2015) through the SAGA database (Suda et al. 2017). The solid line connects the averages of [Mg/Fe] (and [Fe/H]) of the objects in 0.25-dex bins of [Fe/H], and the bar indicates the standard deviations of the [Mg/Fe] values. In the calculations of the averages and standard deviations, the five CEMP stars with Mg excess are excluded.

Although statistically significant scatter exists in the [Mg/Fe] ratios of EMP stars, the large excess of [Mg/Fe] in the five objects with [Fe/H] ~ -4 is distinct. This demonstrates that the five stars are well separated from the bulk of the EMP stars that have [Mg/Fe] $\sim +0.4$ on average.

Figure 3 shows the overall abundance pattern of J2217+2104, and those of three of the other CEMP stars previously reported. HE 2139−5432 is not included in the plot, because the number of elements for which abundance measurements were reported is relatively small. The figure demonstrates that the abundance patterns of the elements between O and Ni of these four stars are very similar, considering the measurement errors of typically 0.2 dex. The similarity of the abundance patterns suggests that the progenitors of these objects, which are expected to be a specific type of supernova explosion of massive stars, are also similar. Before discussing the possible origin of the abundance pattern of these stars, we inspect the abundances of C and N, as well as the neutron-capture elements Sr and Ba.

4.2 C and N abundances

The five objects that show large excesses of Mg and Si identified in the previous subsection also have very high abundance ratios of C/Fe and N/Fe. The C/N abundance ratios are, however, different between stars. The abundance ratios of related elements are given in table 4 for the five objects. The data of HE 1327−2326 are also given for comparison purposes. The overabundance of N is larger than that of C in J2217+5104, CS 22949−037, and

Table 4. Abundance ratios of C, N, O, Na, and Mg.

	$T_{\rm eff}$	log g	[Fe/H]	[C/Fe]	[N/Fe]	[O/Fe]	[Na/Fe]	[Mg/Fe]	[C/N]	[(C + N)/O]	[Na/Mg]	^{12}C/^{13}C
J2217+2104	4500	0.90	−3.93	1.03	2.18	2.12	1.33	1.46	−1.15	−0.53	−0.13	6
CS 22949−037	4958	1.84	−3.97	1.06	2.16	1.98	2.10	1.38	−1.10	−0.40	0.72	4
CS 29498−043	4639	1.00	−3.49	1.90	2.30	2.43	1.47	1.52	−0.40	−0.42	−0.05	6
HE 1012−1540	5745	3.45	−3.47	2.22	1.25	2.25	1.93	1.85	0.97	−0.12	0.08	—
HE 2139−5432	5416	3.04	−4.02	2.59	2.08	3.15	2.15	1.61	0.51	−0.63	−0.06	>15
HE 1327−2326	6180	3.70	−5.76	4.26	4.56	3.70	2.48	1.55	−0.30	0.64	0.93	>5

CS 29498−043, whereas the overabundance of C is larger in the other two stars.

The C and N abundances could be affected by the CN-cycle, but the total abundance of the two elements should be preserved during the process. The total abundances of C and N of all of the five stars are very high ([(C + N)/Fe] $> +1.6$), although the carbon abundances of J2217+2104 and CS 22949−037 ([C/Fe] $\sim +1$) are close to the criterion of CEMP stars.

The ratio of the total abundance of C and N with respect to the O abundance (i.e., [(C + N)/O]) is also given in the table. Interestingly, the (C + N)/O ratios in the five objects are very similar. The average and the standard deviation of the ratios are $\langle$[(C + N)/O]$\rangle = -0.42$ and σ([(C + N)/O]) $= 0.19$, respectively. This suggests that C has been enhanced similarly to O in these objects, and a portion of the enhanced C is transformed into N by the CN-cycle, resulting in a variation between the stars.

The C and N abundances could be affected by the CN-cycle in the progenitors of these objects, which would be massive stars that produced large excesses of Mg and Si. The CN-cycle is, however, also effective in the low-mass red giants that we are currently observing. Indeed, a large fraction of highly evolved red giants with a very low metallicity show very low C and high N abundances ("mixed stars"; Spite et al. 2005). The two objects that have relatively high C/N ratios among the five objects are warmer ($T_{\rm eff} > 5400$ K) than the other three objects (table 4). This suggests that the variation in the C/N ratio could be due to the CN-cycle during the low-mass star evolution. The low ^{12}C/^{13}C ratios in the three cool stars and non-detection of ^{13}C in the others (table 4) support this interpretation.

The [C/O] ratios in metal-poor damped Lyman-α systems are similar to the [(C + N)/O] values of CEMP stars studied here. Cooke, Pettini, and Steidel (2017) argue that the source of the C and O in the systems is supernova explosions of $\sim$20 $M_{\odot}$, based on nucleosynthesis models for first stars, and supernova explosions in which the C/O ratio is sensitive to the mass of progenitors (Heger & Woosley 2010). Constraints on the progenitor mass obtained by elemental abundances are discussed in subsection 4.4.

4.3 Neutron-capture elements

Heavy neutron-capture elements are deficient in EMP stars with [Fe/H] < -3.5 in general, in contrast to objects with [Fe/H] ~ -3 that show large star-to-star scatter in their abundance ratios (e.g., [Eu/Fe]), including r-process-enhanced stars. In EMP stars with low abundances of neutron-capture elements, the only measurable neutron-capture elements that have strong resonance lines in the optical range are Sr and Ba. The [Sr/Fe] and [Ba/Fe] ratios in stars with [Fe/H] < -3.5 are typically -1 (e.g., Yong et al. 2013). Figure 4(A) shows [Ba/Fe] as a function of [Fe/H] for metal-poor stars. CEMP-s stars are excluded from this plot. The [Ba/Fe] values of CEMP stars with excesses of Mg and Si previously reported are not as low as the typical [Ba/Fe] values of other EMP stars with similar Fe abundances. This was discussed by Aoki et al. (2002) for CS 22949−037 and CS 29498−043. J2217+2104 has, however, very low abundances of Sr and Ba, as found in C-normal stars with [Fe/H] < -3.5. This indicates that scatter exists in the abundance ratios of neutron-capture elements in such CEMP stars.

For such CEMP stars, Fe is not necessarily a good indicator of metallicity, because O, Mg, and Si are overabundant with respect to Fe. Figure 4(B) shows [Ba/Fe] as a function of [Mg/H], adopting Mg as an indicator of metallicity. Since the typical value of [Mg/Fe] in metal-poor stars is +0.4, most stars are shifted to higher values in the horizontal axis compared to the plot for [Fe/H]. The large scatter of [Ba/Fe] appears at [Mg/H] ~ -2.6 in this diagram, corresponding to the scatter at [Fe/H] ~ -3 in figure 4(A). On the other hand, CEMP stars with a Mg excess are shifted by more than 1 dex. The [Ba/Fe] values of the two particularly Mg-rich stars ([Mg/H] > -2) are similar to the typical value in other stars, while the other two stars, including J2217+2104, are located within the scatter of [Ba/Fe] found in other stars with [Mg/Fe] ~ -2.6.

This suggests that the neutron-capture elements of CEMP stars with excesses of Mg and Si follow the distribution of neutron-capture elements of other EMP stars showing no C-excess, and there is no direct connection between the origin of excesses of C, N, O, Mg,

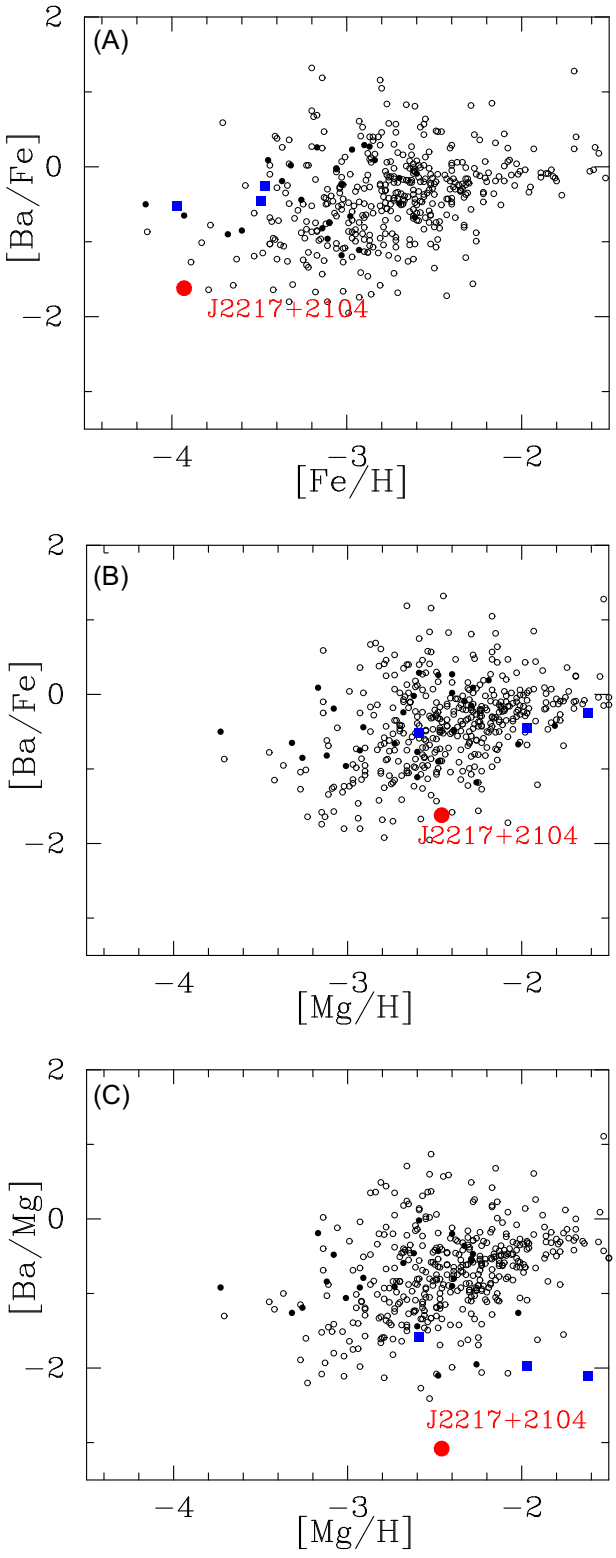

Fig. 4. [Ba/Fe] as a function of [Mg/H]. CEMP stars with excesses of Mg and Si are shown by the red filled circle (J2217+2104) and blue filled squares. Others (small circles) are taken from the literature the same as in figure 2: filled circles are CEMP-no stars and open circles are C-normal stars or those for which C abundances are yet constrained.

and Si and the event that has produced neutron-capture elements.

We note for completeness that, in the plot of [Ba/Mg] as a function of [Mg/H] shown in figure 4(C), the CEMP stars with excesses of Mg and Si are well separated from the other stars, showing very low values of [Ba/Mg]. This is simply due to the large Mg excess.

4.4 Progenitors of CEMP stars with excesses of Mg and Si

The extremely low metallicity (low Fe abundance) of these objects indicates that their elemental abundances would be predominantly determined by the chemical yields of first generation stars. We find 49 objects in the range $-4.5 <$ [Fe/H] < -3.5 in figure 2, out of which five are CEMP stars showing large Mg excesses, suggesting that the frequency of such objects is in the order of 10%. Hence, if the chemical compositions of these stars originate from similar objects, e.g., some specific type of supernova, they should not be very rare in the early Galaxy. We note that the high fraction of CEMP-no stars at very low metallicity might not only reflect the frequency of their progenitors, but also depend on the efficiency of low-mass star formation that is affected by the chemical composition of the gas cloud, as discussed by, e.g., Norris et al. (2013) and Chiaki, Tominaga, and Nozawa (2017).

A promising model proposed to explain the abundance patterns of these objects is the so-called mixing-fallback model for supernova explosions (Umeda & Nomoto 2003). This model assumes significant mixing in the inner region of a massive star during the explosion and unusually large fall-back that results in little ejection of heavier elements including Fe. Abundance patterns predicted by this model have been compared with CEMP stars including CS 22949−037 and CS 29498−043. Recently, Ishigaki et al. (2018) applied the models covering wide ranges of masses and explosion energies to abundance patterns of many EMP stars. They showed that the abundance patterns of CEMP stars with excesses of Mg and Si are better explained by the models of 25 $M_\odot$ rather than by those of more massive cases. This is in particular constrained by the [Na/Mg] ratios. Figure 5 shows the abundance patterns predicted by models for three different progenitor masses (13, 25, and 40 $M_\odot$) for explosion energy of 10^{51} erg along with the abundance ratios of J2217+2104. Here the total abundances of C and N are presented, taking account of possible conversion of C to N by the CN-cycle after nucleosynthesis in a massive progenitor. The abundance pattern of J 2217+2104 from C + N to Ca is well reproduced by the model of 25 $M_\odot$,

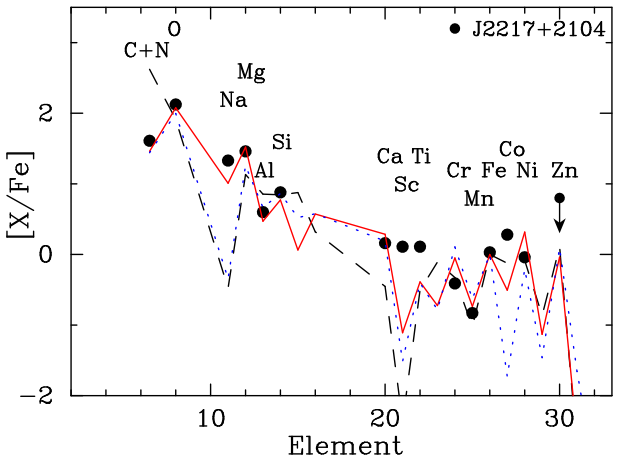

Fig. 5. Abundance pattern of J2217+2104 and predictions by models of Ishigaki et al. (2018) for stellar masses of 13 $M_\odot$ (black dashed line), 25 $M_\odot$ (red solid line), and 40 $M_\odot$ (blue dotted line) with explosion energy of 1.0×10^{51} erg. The ratio of total abundance of C and N to Fe, [(C + N)/Fe], is shown. The model for $M = 25\,M_\odot$ well reproduces the abundance ratios from C + N to Ca. (Color online)

whereas two ratios, (C + N)/Fe and Na/Fe, are not explained by the other models.

The Co/Fe ratio is not well reproduced by any models, and is better explained by models assuming large explosion energies (hypernova cases). However, the [Na/Mg] values, as well as [(C + N)/O] values, of the CEMP stars studied here are better explained by models with a normal explosion energy (10^{51} erg; Ishigaki et al. 2018). The explosion energy is well constrained by the Zn abundance. The Zn abundance of CS 22949−037 reported by Depagne et al. (2002) is [Zn/Fe] = +0.7, suggesting a large explosion energy, whereas the upper limit derived for CS 29498−043 by Aoki et al. (2004) is relatively low ([Zn/Fe] < +0.5) and, hence, a particularly high explosion energy is not required. The upper-limit of the Zn abundance estimated for J2217+2104, [Zn/Fe] < +0.7, is still marginal, and further measurements will provide useful constraints. The high Sc and Ti abundances of J2217+2104 are not reproduced by any models, and the model values are treated as lower limits in the fitting (Ishigaki et al. 2018). The abundances of these two elements, as well as the high Co abundance, could be explained by a jet-induced explosion (Tominaga et al. 2014).

The progenitor mass for these CEMP stars is also estimated to be about 20 $M_\odot$ by supernova models of Heger and Woosley (2010). Placco et al. (2016) compare the models with the abundance pattern of CS 22949−037, which has a similar abundance pattern to J2217+2104, and concluded that the model for 21.5 $M_\odot$ of Heger and Woosley (2010) provides the best fit. The strongest constraint is also given by the abundance ratios of C(+N), O, Na, and Mg.

The initial mass function of first stars is one of the most important issues in understanding early structure formation. It has been constrained by comparisons between models and observations, such as the metallicity distribution function of most metal-poor stars and the fraction of CEMP stars (e.g., de Bennassuti et al. 2017). Estimating the mass of progenitor stars for individual metal-poor stars is another approach to this goal. The mass of the progenitors estimated for CEMP stars with excesses of Mg and Si is not particularly different from that expected for C-normal EMP stars. This suggests that, although the progenitors of such CEMP stars produced C-rich material due to some properties of stars (e.g., rotation, binarity), they could represent some important portion of the initial mass function of first stars.

Significant mass-loss from first-generation (metal-free) massive stars with rapid rotation is also proposed to explain CEMP-no stars, in particular the hyper metal-poor ([Fe/H] < −5) stars showing extremely large excesses of C and other light elements (Meynet et al. 2006). Remarkable features predicted by this model are large excesses of odd elements, i.e., N, Na, and Al, as a result of the CNO-cycle and the efficient mixing caused by rapid rotation. The large excesses of N and Na, as well as C and Mg, found in the CEMP stars discussed here support the model. The N excess might, however, be produced during the evolution of the low-mass stars we are currently observing, as discussed in subsection 4.2. Another difficulty is the excess of Si, which is not expected in the material ejected from rotating massive stars.

Another model proposed as a possible origin of CEMP-no stars is mass transfer from companion AGB stars in binary systems (Suda et al. 2004). Large enhancements of Na and Mg are predicted by a neutron-capture nucleosynthesis model of very metal-poor AGB stars (Nishimura et al. 2009). However, the large excess of Si found in the CEMP stars discussed here is not explained by this model. The [(C + N)/O] ratios observed for the sample of this work are not as high as the C/O ratios expected from AGB nucleosynthesis models. Hence, at least according to the current AGB nucleosynthesis models, mass transfer from AGB stars is implausible as the origin of CEMP-no stars with large excesses of Mg and Si, whereas it could be a possible origin of some portion of other CEMP-no stars.

5 Summary and concluding remarks

The elemental abundances of a newly discovered CEMP star, J2217+2104, are determined based on high-resolution spectroscopy. This is a new example of a class of CEMP stars that have excesses of N, O, Na, Mg, Al, and Si. The abundance patterns of this class of objects from C to Ni are very similar to each other, suggesting the existence of

similar progenitors in the early universe that would be a specific type of supernova explosion. The abundance pattern of C, N, O, Na, and Mg of J2217+2104 and other similar CEMP stars suggests that the progenitor mass is about 25 $M_{\odot}$, which is not particularly different from typical mass of progenitors expected for EMP stars in general. Hence, the cause of the very different abundance pattern of these CEMP stars from other EMP stars would be some property of progenitors other than their mass. The difference comes from the parameters of mixing and fallback in the model (Ishigaki et al. 2018), which might be related to the rotation, binarity, or other properties.

The kinematic information of Galactic stars is becoming available via new astrometry data obtained with Gaia. The sample size of this class is still too small to determine their chemical and kinematic properties and their implication in the early nucleosynthesis and star formation. Ongoing and future surveys of very metal-poor stars will be useful for searching for EMP/UMP stars including such carbon-enhanced objects.

Acknowledgments

This work is based on data collected at the Subaru Telescope, which is operated by the National Astronomical Observatory of Japan. Guoshoujing Telescope (the Large Sky Area Multi-Object Fiber Spectroscopic Telescope, LAMOST) is a National Major Scientific Project built by the Chinese Academy of Sciences. Funding for the project has been provided by the National Development and Reform Commission. LAMOST is operated and managed by the National Astronomical Observatories, Chinese Academy of Sciences. This work was supported by JSPS - CAS Joint Research Program. WA and TS were supported by JSPS KAKENHI Grant Numbers 16H02168, 16K05287, and 15HP7004. MNI was supported by JSPS KAKENHI Grant Number 17K14249. HL was supported by NSFC grants Nos. 11573032, 11390371. We thank Dr. M.Y. Fujimoto for useful comments on AGB nucleosynthesis.

References

Alonso, A., Arribas, S., & Martínez-Roger, C. 1999, A&AS, 140, 261
Aoki, W., et al. 2013, AJ, 145, 13
Aoki, W., Beers, T. C., Christlieb, N., Norris, J. E., Ryan, S. G., & Tsangarides, S. 2007, ApJ, 655, 492
Aoki, W., Norris, J. E., Ryan, S. G., Beers, T. C., & Ando, H. 2002, ApJ, 576, L141
Aoki, W., Norris, J. E., Ryan, S. G., Beers, T. C., Christlieb, N., Tsangarides, S., & Ando, H. 2004, ApJ, 608, 971
Asplund, M., Grevesse, N., Sauval, A. J., & Scott, P. 2009, ARA&A, 47, 481
Barklem, P. S., et al. 2005, A&A, 439, 129
Bonifacio, P., et al. 2018, A&A, 612, A65
Bromm, V., & Loeb, A. 2003, Nature, 425, 812
Castelli, F., Gratton, R. G., & Kurucz, R. L. 1997, A&A, 318, 841
Cayrel, R., et al. 2004, A&A, 416, 1117
Chiaki, G., Tominaga, N., & Nozawa, T. 2017, MNRAS, 472, L115
Cohen, J. G., Christlieb, N., Thompson, I., McWilliam, A., Shectman, S., Reimers, D., Wisotzki, L., & Kirby, E. 2013, ApJ, 778, 56
Cooke, R. J., Pettini, M., & Steidel, C. C. 2017, MNRAS, 467, 802
Cui, X.-Q., et al. 2012, Res. Astron. Astrophys., 12, 1197
Cutri, R. M., et al. 2003, 2MASS All-Sky Catalog of Point Sources, VizieR Online Data Catalog, II/246
de Bennassuti, M., Salvadori, S., Schneider, R., Valiante, R., & Omukai, K. 2017, MNRAS, 465, 926
Depagne, E., et al. 2002, A&A, 390, 187
Frebel, A., et al. 2005, Nature, 434, 871
Frebel, A., Casey, A. R., Jacobson, H. R., & Yu, Q. 2013, ApJ, 769, 57
Frebel, A., & Norris, J. E. 2015, ARA&A, 53, 631
Hansen, T., et al. 2015, ApJ, 807, 173
Heger, A., & Woosley, S. E. 2010, ApJ, 724, 341
Henden, A. A., et al. 2016, VizieR Online Data Catalog, II/336
Honda, S., Aoki, W., Kajino, T., Ando, H., Beers, T. C., Izumiura, H., Sadakane, K., & Takada-Hidai, M. 2004, ApJ, 607, 474
Ishigaki, M. N., Tominaga, N., Kobayashi, C., & Nomoto, K. 2018, ApJ, 857, 46
Ito, H., Aoki, W., Honda, S., & Beers, T. C. 2009, ApJ, 698, L37
Jacobson, H. R., et al. 2015, ApJ, 807, 171
Käppeler, F., Gallino, R., Bisterzo, S., & Aoki, W. 2011, Rev. Mod. Phys., 83, 157
Lai, D. K., Bolte, M., Johnson, J. A., Lucatello, S., Heger, A., & Woosley, S. E. 2008, ApJ, 681, 1524
Li, H., Aoki, W., Zhao, G., Honda, S., Christlieb, N., & Suda, T. 2015, PASJ, 67, 84
Masseron, T., et al. 2014, A&A, 571, A47
McWilliam, A., Preston, G. W., Sneden, C., & Searle, L. 1995, AJ, 109, 2757
Meynet, G., Ekström, S., & Maeder, A. 2006, A&A, 447, 623
Nishimura, T., Aikawa, M., Suda, T., & Fujimoto, M. Y. 2009, PASJ, 61, 909
Noguchi, K., et al. 2002, PASJ, 54, 855
Norris, J. E., et al. 2013, ApJ, 762, 28
Norris, J. E., Ryan, S. G., & Beers, T. C. 2001, ApJ, 561, 1034
Norris, J. E., Ryan, S. G., Beers, T. C., Aoki, W., & Ando, H. 2002, ApJ, 569, L107
Placco, V. M., et al. 2016, ApJ, 833, 21
Ryan, S. G., Norris, J. E., & Beers, T. C. 1999, ApJ, 523, 654
Schlafly, E. F., & Finkbeiner, D. P. 2011, ApJ, 737, 103
Sneden, C., Lucatello, S., Ram, R. S., Brooke, J. S. A., & Bernath, P. 2014, ApJS, 214, 26
Spite, M., et al. 2005, A&A, 430, 655
Suda, T., et al. 2008, PASJ, 60, 1159
Suda, T., et al. 2017, PASJ, 69, 76
Suda, T., Aikawa, M., Machida, M. N., Fujimoto, M. Y., & Iben, I., Jr. 2004, ApJ, 611, 476
Tominaga, N., Iwamoto, N., & Nomoto, K. 2014, ApJ, 785, 98
Umeda, H., & Nomoto, K. 2003, Nature, 422, 871
Yong, D., et al. 2013, ApJ, 762, 26
Yoon, J., et al. 2016, ApJ, 833, 20
Zhao, G., Zhao, Y.-H., Chu, Y.-Q., Jing, Y.-P., & Deng, L.-C. 2012, Res. Astron. Astrophys., 12, 723